Applied Acoustics 148 (2019) 1–8

Contents lists available at ScienceDirect

Applied Acoustics

journal homepage: www.elsevier.com/locate/apacoust

Acoustical siphon effect for reducing the thickness in membrane-type metamaterials with low-frequency broadband absorption

Chong Rui Liu [a,b], Jiu Hui Wu [a,b,*], Kuan Lu [a,b], Zi Ting Zhao [a,b], Zhen Huang [a,b]

[a] School of Mechanical Engineering, Xi'an Jiaotong University, Xi'an 710049, China
[b] State Key Laboratory for Strength and Vibration of Mechanical Structures, Xi'an Jiaotong University, Xi'an 710049, China

ARTICLE INFO

Article history:
Received 22 May 2018
Received in revised form 8 November 2018
Accepted 6 December 2018

Keywords:
Membrane-type metamaterials
Acoustical siphon effect
Low-frequency broadband sound absorption
Absorption coefficient
Acoustic impedance

ABSTRACT

Acoustical siphon effect in membrane-type metamaterials for low-frequency broadband absorption is proposed, whose physical mechanism is further investigated by the theoretical analysis and finite element (FE) simulation. This kind of membrane-type metamaterials consists of multiple detuned units, each of which is composed of two aluminum platelets fasten on a piece of silicone membrane above an air cavity. For the multi-unit metamaterial illuminated by an incident plane wave with certain frequency, there exists a certain unit at resonance with maximum acoustic absorption, and meanwhile other units nearly keep static due to the narrow absorption peak of the resonant unit. Therefore, almost the whole incident energy can be forced to flow to this resonant unit resulting in a much enhanced vibration and a reduced acoustic impedance that could be more matchable to air medium, and thus much more acoustic absorption appears without increasing the unit thickness, which is called acoustical siphon effect of the unit. On this basis, by precisely designing the acoustical siphon effect of each unit, the broadband absorption can be obtained by a subwavelength six-unit sample in the low-frequency range of 400–650 Hz with the maximum absorption coefficient of almost 100% and the average absorption coefficient of about 80%, which is then verified by the corresponding experiment. The results presented here would offer a new approach for the metamaterials design for low-frequency broadband sound absorption and could have potential applications in controlling vibration and noise.

1. Introduction

Recent years have witnessed a rapid development of acoustic metamaterials due to the excellent absorption performance for the low-frequency sound. Compared with the traditional materials [1–5], such as porous materials and perforated or micro-perforated panels, the metamaterials gain smaller structural dimensions and higher energy dissipation efficiency. Up to now, a series of novel metamaterials has been obtained, most of which can achieve 100% absorption with subwavelength thicknesses, including membrane-type metamaterials (MAMs) [6–13], acoustic metasurfaces [14–17], coiling-up space metamaterials [18–21], slow-wave metamaterials [22–25], and Helmholtz resonators [26,27]. Nevertheless, these metamaterials can only gain good sound absorption performance in a narrow frequency range around the resonant frequency, which has been a major obstacle in practical applications. Thus, the achievement of low-frequency broadband absorption performance with a subwavelength thickness becomes one of the current research hotspots and scientific challenges.

To this date, some typical structures have been reported with low-frequency broadband sound absorption achieved by introducing multiple detuned absorption units [28–37]. According to the unit arrangements, these broadband absorption metamaterials can be generally divided into two categories, series arrangements or parallel arrangements. For the series arrangements [28–33], the broadband absorption performance is easily obtainable by placing the new units on the underside of the original structure, but the structure's thickness is sharply increased, which limits the engineering applications. By contrast, the parallel arrangements [34–37], in which the new units are mounted on the lateral side of the original, can provide a better choice for the broadband absorption because the thickness has a lower increase than that of series arrangement. Among these parallel structures, Helmholtz resonators or the perforated plates are usually adopted as the basic absorption units. In fact, the surface acoustic impedance of the parallel structure can be expressed as $Z_0 = Z_i/\eta$, where Z_i is the surface acoustic impedance of a certain unit and η is the absorption area ratio of the absorption unit to the structure. With the acoustic

* Corresponding author.
E-mail address: ejhwu@mail.xjtu.edu.cn (J.H. Wu).

https://doi.org/10.1016/j.apacoust.2018.12.008
0003-682X/

impedance Z_i maintained unchanged, the increased number of the units can lead to a proportional enhancement of the acoustic impedance Z_0 of the structure and a decrease of the absorption coefficient accordingly. Thus, the most common way to achieve satisfactory absorption performance is to increase the thickness of the unit greatly, but which is not beneficial to the optimal structure design and the engineering applications.

Inspired by the previous works and discussions, a new kind of membrane-type metamaterials with a subwavelength thickness is proposed that obtains multiple low-frequency high absorption peaks. The acoustic impedance of a certain membrane-type unit in the multi-unit metamaterials can be further reduced without increasing its thickness, while the peak frequency stays constant. More specifically, the whole incident acoustic energy is forced to flow to the certain unit from the surrounding units due to the surface pressure difference, by which the vibration intensity of the unit is raised and the acoustic impedance Z_i is lowered consequently. The acoustic impedance Z_0 of the multi-unit membrane-type metamaterials therefore does not have such drastic enhancements, showing good robustness and great potential for the broadband absorption. This effect of energy concentration in the near field is defined as the *acoustical siphon effect* here. The peak frequency can be maintained constant since the natural vibration characteristic of the unit is unchanged by the acoustical siphon effect. It can be concluded that the wider band in low-frequency range can be achieved by the MAMs with a thinner thickness, which offers a new perspective for future works. In addition, by thoroughly investigating the generating mechanism and the influences on the absorption properties, the acoustical siphon effect is formally proposed as the basic physical mechanism of broadband absorption in this paper and provides a better physical understanding for the structure design.

The paper is organized as follows: Section 2 introduces the acoustical siphon effect in MAMs and explains the underlying physical mechanism for broadband absorption theoretically. Moreover, the robustness of acoustic impedance under the acoustical siphon effect is discussed; in Section 3, the specific absorption performances of the MAMs with different absorption area ratios are investigated and the effects of the key parameters analyzed in details; in Section 4, a thin MAMs sample with low-frequency broadband sound absorption is obtained, of which the simulation results are verified by the corresponding experiment. Finally, several conclusions are drawn in Section 5.

2. Description and theoretical analysis of the acoustical siphon effect

2.1. The membrane-type metamaterials with the acoustical siphon effect

To illustrate the acoustical siphon effect, Fig. 1 presents two kinds of MAMs with air cavities, wherein MAM 1 consists of one basic unit, and MAM 2 is comprised of two different units obtained by tuning the parameters of the basic unit. The basic unit is composed of three parts: a piece of rectangular silicone membrane, two same semi-circular aluminum platelets and an acoustically rigid frame that builds an air cavity for the unit. The materials parameters used in the calculation are shown in Table 1. The two platelets with a radius of r = 6 mm, a thickness of h = 0.4 mm and a distance of d = 15 mm are fastened on the membrane with width W = 21 mm, the length L = 36 mm and thickness t_0 = 0.2 mm. The membrane's boundary is fixed on the frame with depth H = 30 mm and wall thickness t = 1 mm. Moreover, the membrane is applied with an initial stress $\sigma_x = \sigma_y = 2.2\text{e}5$ Pa. The unit 1 in MAM 2 is a full copy of the basic unit (MAM1). As for unit 2, the platelets have a thickness of h = 2 mm and other parameters are held the same to those of unit 1.

To obtain the acoustic absorption performance of the MAMs, a FE simulation model is developed by using the commercial finite element software, COMSOL Multiphysics™ 5.2, in which the acoustic-solid interaction with geometric nonlinearities is selected. The membranes, platelets and frame are defined as solid domains, while the air cavity is defined as an air domain. A plane incident wave is applied perpendicularly on the surface of the MAMs along the negative direction of the x axis. The fixed boundary conditions are imposed on the outer edges of the membrane in each unit. Material properties and geometrical dimensions are kept the same as those parameters mentioned above. According to the test results [7,8], the damping factor of the membrane is set to $\chi_0\omega$ with χ_0 = 4.2e−4 s that can be expressed as an imaginary part of the Young modulus in the model, i.e. $E = 1.9\ (1 + 4.2\text{e}{-4}\omega i)$ MPa. Besides, the density and sound speed of the air are ρ_0 = 1.29 kg/m^3 and c_0 = 340 m/s, respectively.

The sound absorption of the MAMs is the result of the vibration energy dissipation in the membrane with viscous damping, and the maximum energy dissipation can be obtained at resonance. The sound absorption coefficients and the resonance modes of two MAMs are demonstrated in Fig. 2. It is found that MAM 1 has three high absorption peaks caused by the three different resonance modes: translational motion of the platelets, the strong vibration of the membrane with the rotational motion of the platelets and the vibration of the partial membrane in the center of the unit, while MAM 2 obtains five absorption peaks due to the additional resonance modes provided by unit 2. It is worth noting that, compared with MAM 1, the peak absorption coefficient (about 99%) at f = 470 Hz in MAM 2 remains nearly unchanged with the area ratio η decreasing from 100% to 50%, which is attributed to the acoustical siphon effect. Besides, the frequencies of the absorption peaks resulting from unit 1 are not influenced by the new unit (unit 2) in MAM 2.

The distributions of the air particle velocities in MAM 2 at f = 470 Hz are illustrated in Fig. 3(a), from which most of the incident energy is "attracted" to unit 1 from the surrounding area due to the surface pressure difference between unit 1 and unit 2. Therefore the translational motion of the platelets of unit 1 in MAM 2 is enhanced with the acoustical siphon effect compared with that in MAM 1. This can be verified in Fig. 2(b) and (c) when the displacement amplitude of unit 1 is raised from 3e−3 mm to 4e−3 mm. Particularly, the corresponding elastic curvature energy shown in Fig. 3(b), which is proportional to the energy dissipated in unit 1, is increased by about 2 times. It can be concluded that the acoustic energy absorbed by MAM 2 is approximately doubled, and therefore the peak absorption coefficient (f = 470 Hz) can be kept unchanged when the unit area ratio decreases by half. Though the vibration intensity is enhanced by the acoustical siphon effect, the natural vibration characteristic is not changed and the peak frequencies can remain constant. In later sections, the specific discussions on the impedance characteristics of the MAMs will be conducted.

2.2. Physical mechanism of the acoustical siphon effect

As mentioned above, the acoustical siphon effect is generated by the surface pressure difference resulting from the inhomogeneity of the acoustic impedance. In this section, a simple theoretical analysis is conducted to interpret the generating mechanism of the acoustical siphon effect.

As shown in Fig. 4(a), the sound absorption structure is assumed to consist of two units: unit A and unit B, of which the surface acoustic impedances and the absorption peak frequencies

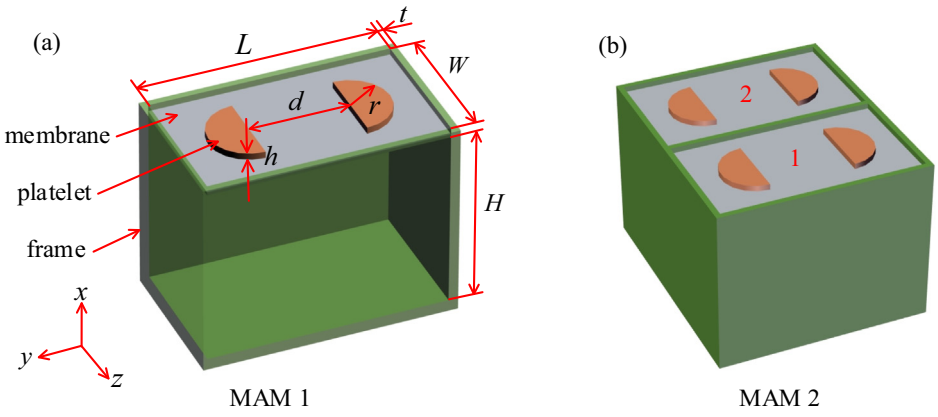

Fig. 1. Schematic diagrams of the two MAMs. (a) MAM 1 is composed of a basic unit: the width and length of the membrane: W = 21 mm, L = 36 mm, the radius, the thickness and the distance of the platelets: r = 6 mm, h = 0.4 mm and d = 15 mm, the depth of the frame (air cavity) H = 30 mm, and the frame's wall thickness t = 1 mm; (b) MAM 2 is composed of two units: unit 1 is a full copy of MAM 1 and unit 2 remains the same as unit 1 with the exception of the thickness of the platelets: h = 2 mm.

Table 1
Materials parameters used in the calculation.

Material	Mass density ρ(kg/m^3)	Young modulus E (MPa)	Poisson's ratio v
Silicone membrane	980	1.9	0.48
Aluminum platelet	2700	72,000	0.35

are Z_A, Z_B, f_A and f_B, respectively. The acoustic impedances Z_A and Z_B are expressed as

$$\begin{cases} Z_A = R_A + jX_A \\ Z_B = R_B + jX_B \end{cases}, \tag{1}$$

where R_A, R_B, X_A and X_B are the acoustic resistances and the acoustic reactance of the two units, respectively.

While a plane wave is applied perpendicularly on the structure surface from the region $x < 0$, the incident sound pressure field P_i and the reflected sound pressure field P_r can be written as

$$\begin{cases} P_i = p_{ia}\exp[j(\omega t - kx)], \\ P_r = \gamma p_{ia}\exp[j(\omega t + kx + \sigma\pi)], \end{cases} \tag{2}$$

where p_{ia} is the amplitude of the incident sound pressure, $j = \sqrt{-1}$ is the imaginary unit, ω is the angular frequency, k is the wave number, γ is the magnification coefficient of the amplitude of the incident sound pressure and $\sigma\pi$ is the phase difference between the incident wave and the reflected wave. The total sound pressure field P is therefore given by

$$P = p_{ia}\exp(j\omega t)[\exp(-jkx) + \gamma\exp(jkx + \sigma\pi)], \tag{3}$$

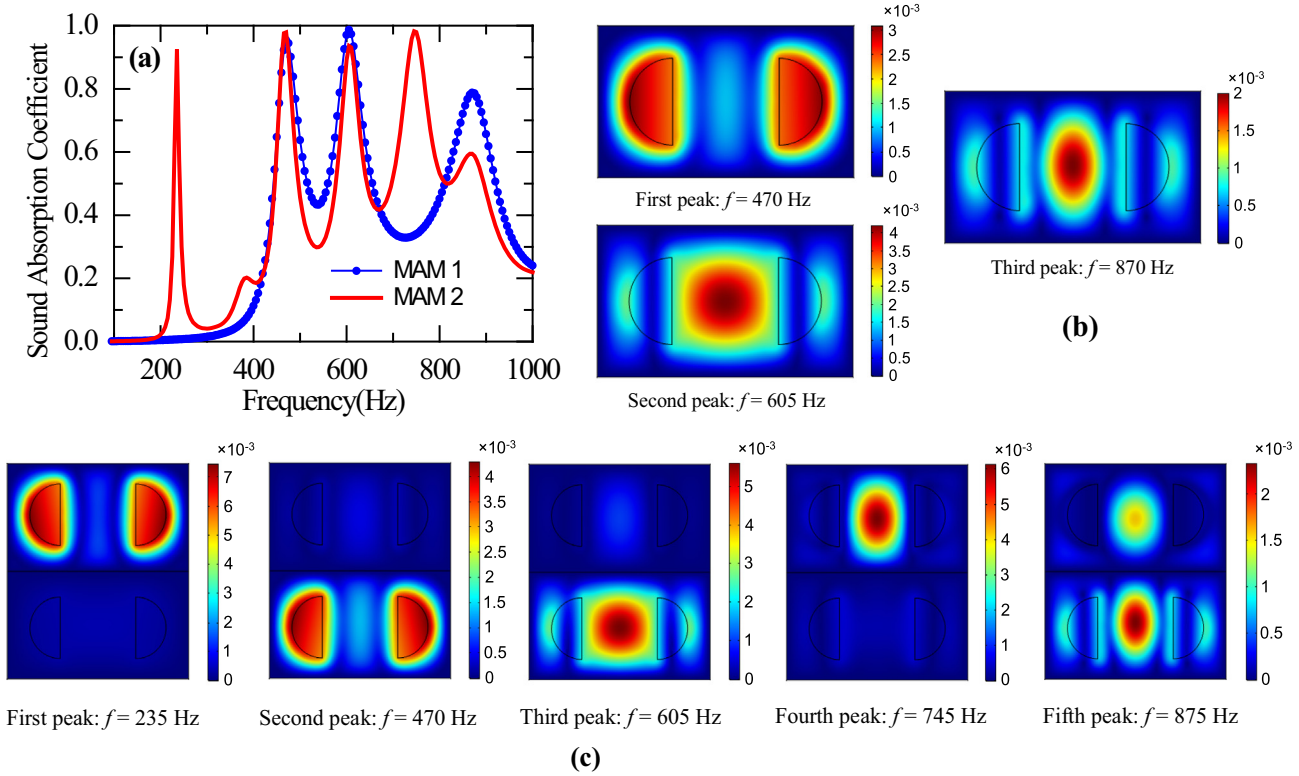

Fig. 2. (a) Sound absorption coefficients of MAM 1 and MAM 2; resonance modes and displacement amplitudes of (b) MAM 1, (c) MAM 2 at absorption peak frequencies.

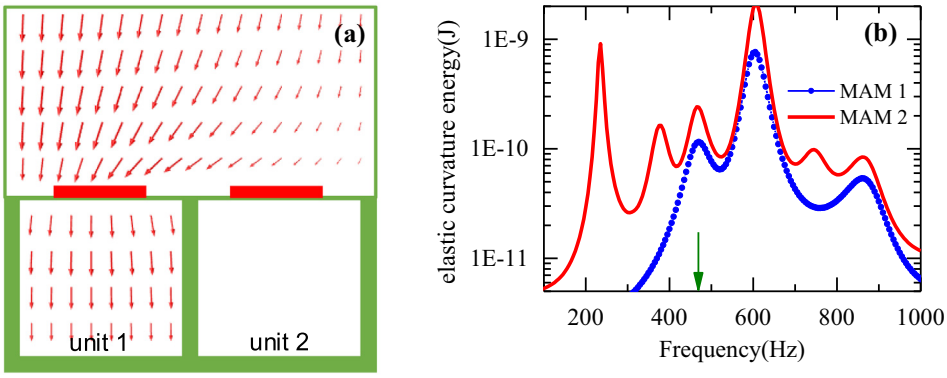

Fig. 3. (a) Acoustical siphon effect in MAM 2 at $f = 470$ Hz expressed with the distribution of the air particle velocity; (b) elastic curvature energy of both MAM 1 and MAM 2 with the green arrow at $f = 470$ Hz. (For interpretation of the references to colour in this figure legend, the reader is referred to the web version of this article.)

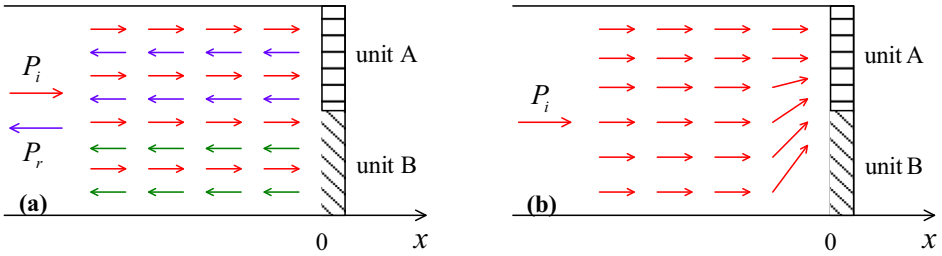

Fig. 4. (a) Air motion without acoustical siphon effect; (b) air motion with acoustical siphon effect.

and the air particle velocity is obtained as

$$v(x,t) = p_{ia}\exp(j\omega t)[\exp(-jkx) - \gamma\exp(jkx + \sigma\pi)]/\rho_0 c_0, \tag{4}$$

where $\rho_0 c_0$ is the characteristic impedance of the air. Using Eqs. (1), (3) and (4), we have

$$\begin{cases} \gamma_{A,B} = sqrt\left[\dfrac{(R_{A,B}-1)^2 + X_{A,B}}{(R_{A,B}+1)^2 + X_{A,B}}\right], \\ (\sigma\pi)_{A,B} = \arctan\dfrac{2X_{A,B}}{R_{A,B}^2 + X_{A,B}^2 - 1}, \end{cases} \tag{5}$$

and the surface pressures of unit A and unit B are expressed as

$$\begin{cases} P_A(x=0,t) = p_{ia}\exp(j\omega t)\left[1 + \gamma_A\exp\left((\sigma\pi)_A\right)\right]. \\ P_B(x=0,t) = p_{ia}\exp(j\omega t)\left[1 + \gamma_B\exp\left((\sigma\pi)_B\right)\right]. \end{cases} \tag{6}$$

Finally, the surface sound pressure difference Δp between unit A and unit B is attained as

$$\Delta p = p_{ia}\exp(j\omega t)\left[\gamma_A\exp\left((\sigma\pi)_A\right) - \gamma_B\exp\left((\sigma\pi)_B\right)\right]. \tag{7}$$

It is the surface pressure difference that leads to the air motion and induces the acoustical siphon effect, as shown in Fig. 4(b).

By taking MAM 2 for example, while the sound wave at $f = 470$ Hz is incident to the surface, unit 1 nearly meets the impedance match condition with $R_1 \approx 1$ and $X_1 \approx 0$, and unit 2 can be regarded as a rigid wall with $R_2 \approx \infty$ and $X_2 \approx 1$ since the incident wave is nearly completely reflected. The surface pressure difference between unit 1 and unit 2 can be obtained accordingly from Eqs. (5) and (7), as

$$\Delta p = -p_{ia}\exp(j\omega t). \tag{8}$$

Owing to this pressure difference, the incident energy is forced to flow to unit 1 in MAM 2 from the surrounding area and more energy is absorbed by the enhanced vibration.

It can be concluded that, only with the phenomenon of energy flow in the acoustical siphon effect, the incident wave can be fully absorbed without generating a reflected wave and the excellent absorption performance can be achieved in multi-unit structures consequently. Therefore, the acoustical siphon effect can be used as the basic physical mechanism for broadband absorption.

2.3. The robustness of acoustic impedance under the acoustical siphon effect

The robustness of acoustic impedance is that the acoustic impedance Z_0 of the multi-unit MAMs is not sensitive to the variation of the absorption area ratio η and does not have a proportional enhancement due to the acoustical siphon effect when the absorption area ratio is reduced. The analysis of the robustness is conducted as follows.

The theoretical model of a single unit impedance is analyzed with a simplified schematic diagram shown in Fig. 5. The surface acoustic impedance of the unit is $Z_A = Z_M + Z_c$, where Z_M, Z_c are the acoustic impedances of the membrane-platelets system and the air cavity, respectively. The membrane-platelets system can be equivalent to a mass-spring system [38], of which the acoustic impedance is given by

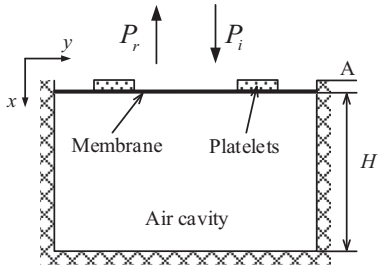

Fig. 5. The simplified schematic diagram of the MAMs unit.

$$Z_M = \left[R + j\left(\omega M - \frac{K}{\omega}\right)\right] \Big/ 2, \tag{9}$$

where R is the equivalent viscous damping of the membrane determined by the vibration intensity, M is the mass of the platelets and membrane, and K is the stiffness depending on the membrane's tension. Since the cavity depth is much smaller than the wavelength, the acoustic impedance of the air cavity can be expressed as

$$Z_c = -i\rho_0 c_0 \cot(kH) \approx -j\rho_0 c_0 / kH. \tag{10}$$

The surface acoustic impedance is therefore written as

$$Z_A = \left[R + j\left(\omega M - \frac{K + 2\rho_0 c_0^2/H}{\omega}\right)\right] \Big/ 2. \tag{11}$$

Then the acoustic impedance of the multi-unit MAMs can be accordingly calculated as $Z_0 = Z'_A/\eta$, where Z'_A is the acoustic impedance of a certain unit in the MAMs. In fact, the vibration velocities of the platelets and membrane of the unit in the multi-unit MAMs are enhanced by the acoustical siphon effect while the incident sound pressure is kept constant. Thus, it is established that the unit impedance is $|Z'_A| < |Z_A|$ from the definition of the acoustic impedance (i.e. $|Z| = |\bar{p}|/|\bar{v}|$, where $|\bar{p}|$ and $|\bar{v}|$ are the amplitudes of the incident sound pressure and the mean vibration velocity of the structure surface, respectively). This can be further verified by the theory of a single-degree-of-freedom system in which a stronger vibration of the system implies a lower equivalent damping, i.e. $R' < R$. Therefore, the surface acoustic impedance of the multi-unit MAMs can be obtained as

$$Z_0 = \left[R' + j\left(\omega M - \frac{K + 2\rho_0 c_0^2/H}{\omega}\right)\right] \Big/ 2\eta, \tag{12}$$

and the sound absorption coefficient is given by

$$\alpha = \frac{4\rho_0 c_0 Z_{re}}{(Z_{re} + \rho_0 c_0)^2 + Z_{im}^2}, \tag{13}$$

where Z_{re} and Z_{im} are the real and imaginary parts of Z_0, respectively. It is known that 100% absorption can be achieved only with $Z_{re} = \rho_0 c_0$ and $Z_{im} = 0$.

Compared with non-MAMs structures (such as Helmholtz resonators and perforated plates), the robustness of the acoustic impedance in MAMs can help to gain lower acoustic impedance without increasing the unit thickness, which is of great value to the design of compact structures for broadband absorption. The specific acoustic impedance characteristics and the sound absorption coefficients are further studied using the FE simulation.

3. Investigation of sound absorption performances with the acoustical siphon effect

In this section, the sound absorption performances of MAMs with the acoustical siphon effect are investigated in detail to offer guidance for the following structure design for broadband absorption.

3.1. Specific sound absorption performances with different absorption area ratios

The investigation is conducted in the FE simulation by changing the frame thickness t in MAM 1. The absorption area ratio to the whole incident area is defined as $\eta = WL/[(W + 2t)(L + 2t)]$, which is selected to vary as 1/2, 1/4, 1/6 and 1/8. The area ratio of MAM 1 is about $\eta = 1$ while the wall thickness is kept unchanged.

Fig. 6(a) and (b) present the absorption coefficients with varied area ratios. It can be seen that the first peak can still be maintained at about 75% as the area ratio is decreased to 1/6, which implies good robustness under the acoustical siphon effect and is of great value to the achievement of the broadband absorption. Besides, the absorption performances of other two peaks are not as efficient as that of the first peak, especially, the third peak that is reduced dramatically and nearly loses absorption ability. Thus, the first absorption peak is the primary option to be adopted for the broadband absorption.

Fig. 6(c) demonstrates the comparison of the absorption performances between the first peak in MAM 1 and the non-MAMs structures in which the unit impedance Z_i cannot be changed by the acoustical siphon effect. The relative impedance $Z_{0r} = Z_0/\rho_0 c_0$ of MAM 1 is extracted from the FE model according to the definition of the acoustic impedance, meanwhile, the relative reactance of the first peak is supposed to $\mathrm{Im}(Z_{0r}) \approx 0$ since the membrane-platelet system is in resonance state. For comparison, the absorption coefficient of the non-MAMs structure is first assumed to be equal to that of MAM1 (about 99%) when the absorption area ratio is $\eta = 1$. The non-MAMs structure therefore should have the same relative impedance as MAM1, i.e. $Z_{non-MAMs} = Z_{0r}(\mathrm{Re}(Z_{non-MAMs}) = 0.8, \mathrm{Im}(Z_{non-MAMs}) = 0)$. The relative impedance of the non-MAMs structure with varied absorption area ratios can be then understood as $\mathrm{Re}(Z_{non-MAMs}) = 0.8/\eta$, and $\mathrm{Im}(Z_{non-MAMs}) = 0$. The corresponding absorption coefficients are derived from Eq. (13). It can be easily found that the MAMs performance has a better robustness than that of the non-MAMs structures as the area ratio is reduced. Due to the acoustical siphon effect, the acoustic impedance in MAMs has a 36% lower amplification than that in the non-MAMs structure as the area ratio is decreased from 1 to 1/8. As a result, the reduction of the sound absorption coefficient in the MAMs structure is about 30% less than that in non-MAMs structure. It can be concluded that the robustness of the absorption performance in the MAMs can help to decrease the thickness of the structure to a certain degree, which is very beneficial to practical applications. In addition, the acoustic impedance of MAM 1 with $\eta = 1$ (the basic unit) should be further reduced to gain lower impedances and better absorption performances when the absorption area ration η is 1/6 or lower.

3.2. Effects of the key parameters on the sound absorption performances

The effects of the key parameters on the sound absorption performances and the impedance characteristics are investigated by the FE model of MAM 1 with the absorption area ratio $\eta = 1/6$, including the depth H of the air cavity, the thickness h of the platelets and the initial stress σ of the membrane.

Fig. 7(a) illustrates the effects of the air cavity depth H on the sound absorption performance of MAM 1, and H is varied sequentially as 20 mm, 30 mm, 40 mm and 50 mm. It can be observed that the air cavity depth has a greater influence on the first absorption peak that is enhanced from 40% to 95% as H increases from 20 mm to 50 mm. This is because the unit impedance is reduced with the increasing depth, which can be verified in Fig. 7(b). The relative acoustic resistance $\mathrm{Re}(Z_0/Z_{air})$ of MAM1 with the area ratio $\eta = 1/6$ is approximately decreased from 3 to 1.55 while H increases from 30 mm to 50 mm, and the absorption coefficient is enhanced to 95% accordingly. Noticeably, the absorption coefficient with a lower area ratio can be raised by the larger depth. Furthermore, the sound absorption coefficient of MAM1 with H = 50 mm remains above 80% as the area ratio is reduced from 1 to 1/8, showing better robustness than that with H = 30 mm.

The effects of the thickness h of the platelets on the sound absorption performance of MAM 1 are shown in Fig. 7(c), with h selected as 0.2 mm, 0.4 mm, 0.8 mm and 1 mm. The cavity depth

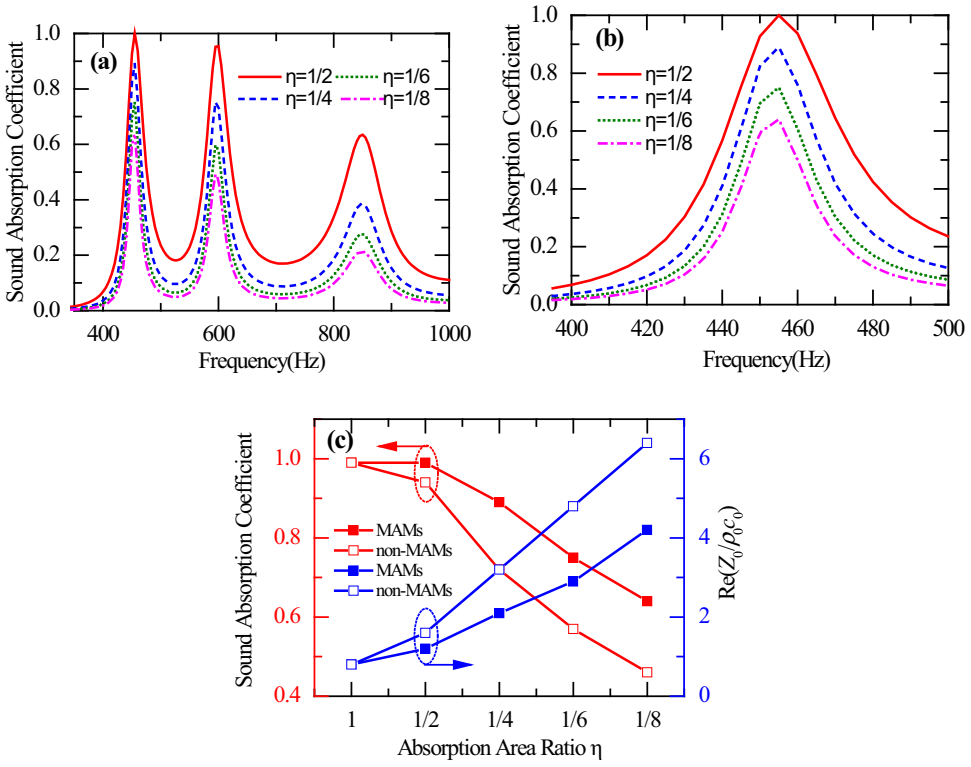

Fig. 6. Absorption performances of (a) MAM 1 and (b) the first peak of MAM 1 with different absorption area ratios achieved by tuning the wall thickness of the frame; (c) comparison of the sound absorption coefficients and the acoustic impedances between the first peak of MAM 1 and non-MAMs structure with different absorption area ratios.

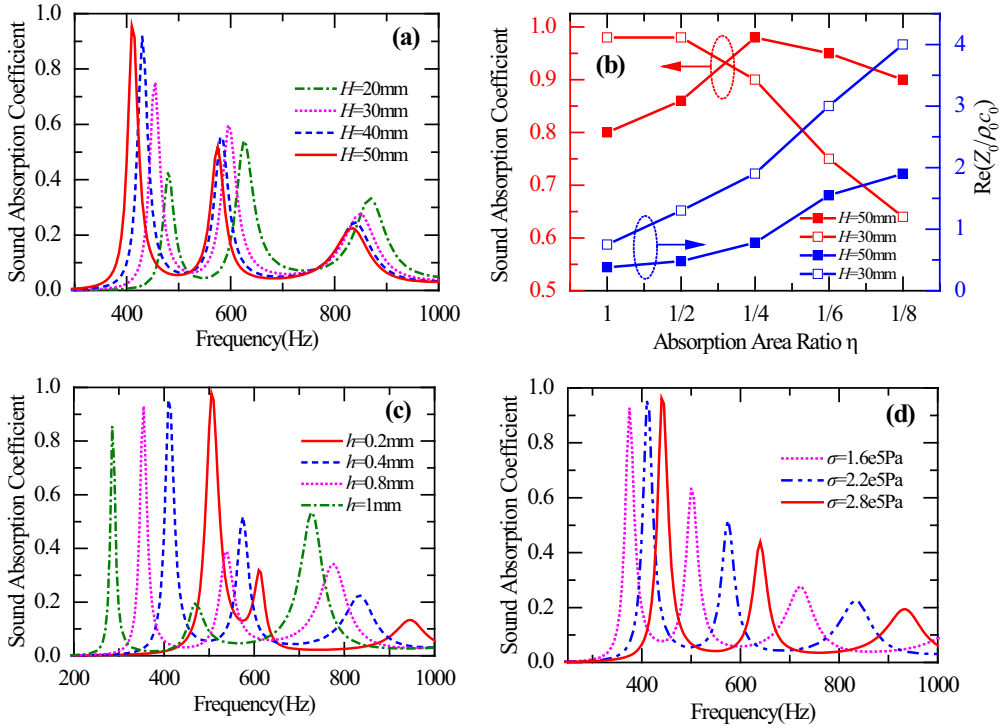

Fig. 7. Effects of key parameters of (a) the depth H of the air cavity, (c) the thickness h of the platelets and (d) the initial stress σ of the membrane on the sound absorption performances of MAM 1 with the absorption area ratio of $\eta = 1/6$; (b) comparison of the specific sound absorption coefficients and the acoustic impedances of MAM 1 with different absorption area ratios between the depth of H = 50 mm and H = 30 mm.

is set to $H = 50$ mm. It can be found that the platelet thickness (i.e. weight) has a stronger effect on the peak frequencies. The three peaks are shifted to lower frequencies markedly as h is increased, which is beneficial for the low-frequency sound absorption. The research is still focused on the first peak that just decreases a little with the increase in thickness.

Fig. 7(d) shows the effects of the initial stress σ of the membrane on the sound absorption performance of MAM 1, with σ varying from 2.8e5 Pa to 1.6e5 Pa and $H = 50$ mm. It can be observed that the three peaks shift to lower frequencies as σ is reduced. More importantly, the absorption coefficient of the first peak, basically, remains unchanged and the other two peaks are enhanced. Thus, the appropriate decrease of the initial stress is of great benefit to the low-frequency absorption.

According to the analysis of the key parameters on the sound absorption performances, the optimal parameters of the structure can be obtained for the low-frequency broadband absorption in practical applications.

4. The low-frequency broadband absorption with the acoustical siphon effect

For low-frequency broadband absorption, a MAMs sample is designed with six critically coupled units, as shown in Fig. 8(a). The diameter and thickness of the sample are 99 mm and 50 mm, respectively. The parameters of each unit are kept the same with those of the basic unit except for the platelet thickness h and the air cavity depth H. The specific parameters of the units are displayed in Table 2. The sample frame is fabricated by the 3D technique with ABS plastics and has a wall thickness of $t = 1.5$ mm between the units that is acoustically rigid and can separate the adjacent units. To verify the results of the FE simulations, the experimental measurements of the sound absorption coefficient are performed by employing the B&K type−4206 impedance tube system. The test sample is installed at the end of the measurement tube and measured with the two-microphone transfer function method [39]. By analyzing the signals of the microphones, the absorption coefficient can be obtained by $\alpha = 1 - |r|^2$ with r representing the reflection coefficient. The sound absorption coefficients between the experimental and simulation results are compared in Fig. 8(b).

Fig. 8(b) shows a continuous broad absorption band in the low-frequency range of 400–650 Hz with the maximum absorption coefficient of almost 100% and the average absorption coefficient of about 80%. The absorption band is actually comprised of seven high absorption peaks contributed by the six units, in which the seventh peak in frequency results from the second vibration mode of each unit. There is a slight difference between the FE simulations and experimental results, mainly because the membrane initial stress is difficult to control accurately by hand. Moreover, the manufacturing errors of the frame and the platelets can also affect the absorption performance. Therefore, it can still be concluded that the MAMs sample has the excellent broadband absorption ability for low-frequency sound. The MAMs with a wider and higher absorption band can be achieved by adopting more units of larger thickness without regard for the limits of structural size caused by the experimental equipment.

5. Conclusions

In this study, the acoustical siphon effect in multi-unit MAMs is proposed and investigated in details, in which almost the whole incident energy is forced to flow to a certain unit from the surrounding area resulting in a much enhanced unit vibration and a decreased unit impedance. Therefore much more absorption can be obtained without increasing the unit thickness. By precisely designing the acoustical siphon effect of each unit, excellent low-frequency broadband absorption is achieved in a 50 mm-thick six-unit sample in the low-frequency range of 400–650 Hz with the maximum absorption coefficient of almost 100% and the average absorption coefficient of about 80%. The absorption performance can be enhanced further with more units and larger thickness without the restrictions of test conditions. Overall, this study would offer an effective guidance for the design of low-frequency broadband sound absorption structures and shows great potential for noise control.

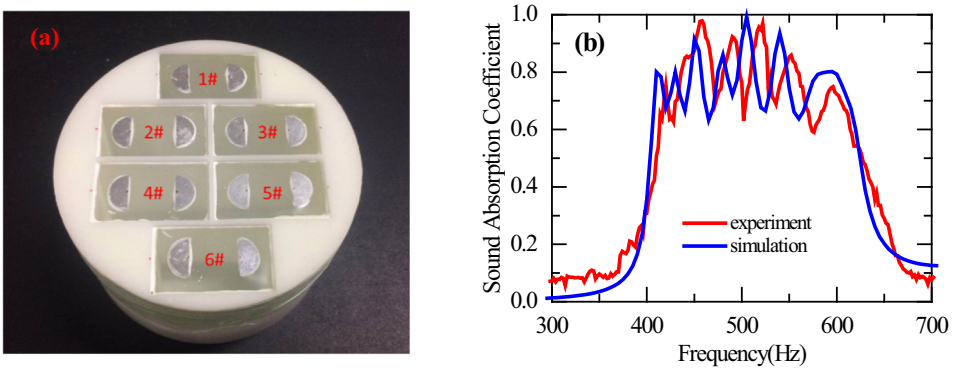

Fig. 8. (a) The MAMs sample with the diameter of 100 mm; (b) comparison of the sample's sound absorption coefficients between the experimental and the FE simulation results.

Table 2
Specific parameters of the sample.

Unit	1#	2#	3#	4#	5#	6#
h (mm)	0.3	0.2	0.4	0.2	0.4	0.3
H (mm)	38	38	40	50	50	50

Acknowledgment

This work was supported by the National Natural Science Foundation of China (NSFC) under Grant No. 51675401.

References

[1] Arenas JP, Crocker MJ. Recent trends in porous sound-absorbing materials. Sound Vib 2010;44(7):12–7.
[2] Maa D-Y. Potential of microperforated panel absorber. J Acoust Soc Am 1998;104(5):2861–6.
[3] Fuchs HV, Zha X. Micro-perforated structures as sound absorbers – A review and outlook. Acta Acust United Acust 2006;92(1):139–46.
[4] Maa DY. Practical single MPP absorber. Int J Acoust Vib 2007;12(1):3–6.
[5] Liu J, Herrin DW. Enhancing micro-perforated panel attenuation by partitioning the adjoining cavity. Appl Acoust 2010;71(2):120–7.
[6] Yang Z, Mei J, Yang M, Chan NH, Sheng P. Membrane-type acoustic metamaterial with negative dynamic mass. Phys Rev Lett 2008;101(20):204301–4.
[7] Mei J, Ma G, Yang M, Yang Z, Wen W, Sheng P. Dark acoustic metamaterials as super absorbers for low-frequency sound. Nat Commun 2012;3(2):756–7.
[8] Chen Y, Huang G, Zhou X, Hu G, Sun C-T. Analytical coupled vibroacoustic modeling of membrane-type acoustic metamaterials: Plate model. J Acoust Soc Am 2014;136(6):2926–34.
[9] Langfeldt F, Riecken J, Gleine W, Von Estorff O. A membrane-type acoustic metamaterial with adjustable acoustic properties. J Sound Vib 2016;373:1–18.
[10] Ma G, Yang M, Xiao S, Yang Z, Sheng P. Acoustic metasurface with hybrid resonances. Nat Mater 2014;13(9):873–8.
[11] Ma F, Huang M, Wu JH. Acoustic metamaterials with synergetic coupling. J Appl Phys 2017;122(21):215102–8.
[12] Leblanc A, Lavie A. Three-dimensional-printed membrane-type acoustic metamaterial for low frequency sound attenuation. J Acoust Soc Am. 2017;104(6):EL538–42.
[13] Ba A, Lavie A, Leblanc A. Soft 3D printed membrane-type acoustic metamaterials. Proc. 23rd Int. Congr. Sound Vib.; 2016 July 10-14; Athens, Greece.
[14] Li Y, Assouar BM. Acoustic metasurface-based perfect absorber with deep subwavelength thickness. Appl Phys Lett 2016;108(6):204301.
[15] Li J, Wang W, Xie Y, Popa BI, Cummer SA. A sound absorbing metasurface with coupled resonators. Appl Phys Lett 2016;109(9):12.
[16] Dubois M, Shi C, Wang Y, Zhang X. A thin and conformal metasurface for illusion acoustics of rapidly changing profiles. Appl Phys Lett 2017;110(15):151902–5.
[17] Schwan L, Umnova O, Boutin C. Sound absorption and reflection from a resonant metasurface: Homogenisation model with experimental validation. Wave Motion 2017;72:154–72.
[18] Cai X, Guo Q, Hu G, Yang J. Ultrathin low-frequency sound absorbing panels based on coplanar spiral tubes or coplanar Helmholtz resonators. Appl Phys Lett 2014;105(12):121901–4.
[19] Wu X, Fu C, Li X, Meng Y, Gao Y, Tian J, et al. Low-frequency tunable acoustic absorber based on split tube resonators. Appl Phys Lett 2016;109(4):043501–43505.
[20] Li Y, Liang B, Tao X, Zhu XF, Zou XY, Cheng JC. Acoustic focusing by coiling up space. Appl Phys Lett 2012;101(23):233508–15.
[21] Xie Y, Konneker A, Popa BI, Cummer SA. Tapered labyrinthine acoustic metamaterials for broadband impedance matching. Appl Phys Lett 2013;103(20):201906–14.
[22] Jiménez N, Huang W, Romero-García V, Pagneux V, Groby JP. Ultra-thin metamaterial for perfect and quasi-omnidirectional sound absorption. Appl Phys Lett 2016;109(12):121902–4.
[23] Groby JP, Huang W, Lardeau A, Aurégan Y. The use of slow waves to design simple sound absorbing materials. J Appl Phys 2015;117(12):124903–9.
[24] Jiménez N, Romero-García V, Pagneux V, Groby JP. Quasiperfect absorption by subwavelength acoustic panels in transmission using accumulation of resonances due to slow sound. Phys Rev B 2017;95(1):014205–14210.
[25] Deng YQ, Qi DX, Tuo MJ, Liu LZ, Zhang RL, Peng RW, et al. Multimode acoustic transparency and slow sound effects in hybrid subwavelength resonators. Appl Phys Express 2017;10:037302–37304.
[26] Long H, Cheng Y, Tao J, Liu X. Perfect absorption of low-frequency sound waves by critically coupled subwavelength resonant system. Appl Phys Lett 2017;110(2):023502–23504.
[27] Cai C, Mak CM. Acoustic performance of different Helmholtz resonator array configurations. Appl Acoust 2018;130:204–9.
[28] Chen C, Du Z, Hu G, Yang J. A low-frequency sound absorbing material with subwavelength thickness. Appl Phys Lett 2017;110(22):221903–4.
[29] Long H, Cheng Y, Liu X. Asymmetric absorber with multiband and broadband for low-frequency sound. Appl Phys Lett 2017;111(14):143502–5.
[30] Groby J-P, Pommier R, Aurégan Y. Use of slow sound to design perfect and broadband passive sound absorbing materials. J Acoust Soc Am 2016;139(4):1660–712.
[31] Yang J, Lee JS, Kim YY. Multiple slow waves in metaporous layers for broadband sound absorption. J Phys D Appl Phys 2017;50(1):015301–15309.
[32] Zhu X, Chen Z-B, Jiao Y, Wang Y. Broadening of the sound absorption bandwidth of the perforated panel using a membrane type resonator. J Vib Acoust 2018;140(3):031014–31016.
[33] Park SH. Acoustic properties of micro-perforated panel absorbers backed by Helmholtz resonators for the improvement of low-frequency sound absorption. J Sound Vib 2013;332(20):4895–911.
[34] Tang Y, Ren S, Meng H, Xin F, Huang L, Chen T, et al. Hybrid acoustic metamaterial as super absorber for broadband low-frequency sound. Sci Rep 2017;7:43340–410.
[35] Jiménez N, Romero-García V, Pagneux V, Groby JP. Rainbow-trapping absorbers: broadband, perfect and asymmetric sound absorption by subwavelength panels for transmission problems. Sci Rep 2017;7:13395–412.
[36] Zhang C, Hu X. Three-dimensional single-port labyrinthine acoustic metamaterial: perfect absorption with large bandwidth and tunability. Phys Rev Appl 2016;6(6):064025–64028.
[37] Jiang X, Liang B, Li RQ, Zou XY, Yin LL, Cheng JC. Ultra-broadband absorption by acoustic metamaterials. Appl Phys Lett 2014;105(24):243505–15.
[38] Fahy F, Gardonio P. Sound and structural vibration; Radiation, Transmission and Response. 2nd ed. Oxford: Academic Press; 2007. p. 278–80.
[39] ISO 10534-2. Acoustics – determination of sound absorption coefficient and impedance in impedance tubes – part 2: transfer-function method; 1998.